Check for updates

Potential low-cost carbon-based adsorbent from gold mine tailings for anionic dye removal

Suheyl Erturk, Muge Sari Yilmaz and Sabriye Piskin

ABSTRACT

In this study, a mesoporous carbon (CMK-3) was successfully synthesized using mesoporous silica (SBA-15) prepared from gold mine tailings (sample C_{GMT}) for removal of anionic dye from aqueous solution. For comparison, CMK-3 was prepared by the same method from pure silica (sample C_T), and the other CMK-3 sample was prepared by a one-pot route mixing with Pluronic P123 (sample C_P). The effect of the carbonization time on the synthesis of all CMK-3 samples was investigated, and the samples were characterized by X-ray diffraction and N_2 adsorption–desorption. The sample with the highest surface area was chosen as an adsorbent, for each CMK-3 obtained from different methods. Batch adsorption experiments were studied to determine the influence of pH, contact time, and initial dye concentration. The adsorption kinetics obeyed the pseudo-second-order model. All carbon-based adsorbents were observed to be quite effective for the removal of dye with adsorption percentage in the order of $C_P > C_T > C_{GMT}$. The maximum adsorption capacities were 188.99 and 204.57 $mg \cdot g^{-1}$ for C_T and C_{GMT}, respectively. The comparative results of all carbon-based adsorbents show that C_{GMT} can be applied as a low-cost alternative to C_T for dye removal.

Key words | CMK-3, dye adsorption, gold mine tailings, low-cost adsorbent, recycling waste

Suheyl Erturk
Muge Sari Yilmaz (corresponding author)
Sabriye Piskin
Faculty of Chemical and Metallurgical Engineering,
Yıldız Technical University,
İstanbul,
Turkey
E-mail: *mugesari@yildiz.edu.tr*

HIGHLIGHTS

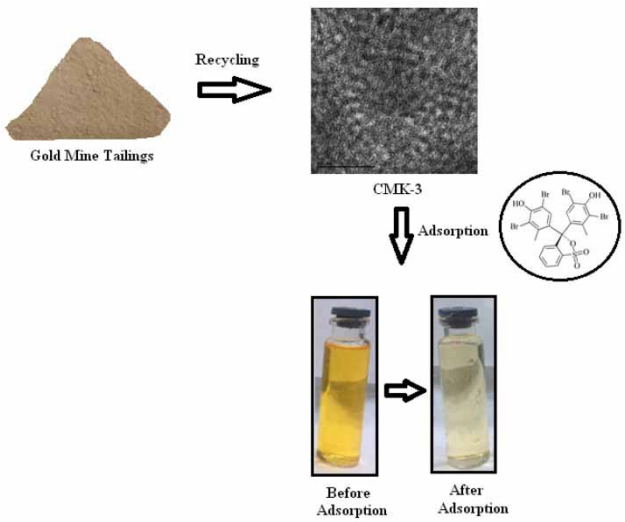
- CMK-3 was synthesized from gold mine waste (C_{GMT}) for the first time.
- The usage of C_{GMT} as low-cost adsorbent for the removal of dye was investigated.
- For comparison, other adsorbents synthesized from different methods were investigated as an adsorbent in the dye adsorption.
- The specific surface area, pore volume and pore size dominate the adsorption capacity.
- C_{GMT} can be applied as a novel, low-cost and alternative adsorbent for dye removal.

This is an Open Access article distributed under the terms of the Creative Commons Attribution Licence (CC BY 4.0), which permits copying, adaptation and redistribution, provided the original work is properly cited (http://creativecommons.org/licenses/by/4.0/).

doi: 10.2166/wst.2021.052

Downloaded from http://iwaponline.com/wst/article-pdf/83/6/1300/865247/wst083061300.pdf
by guest

GRAPHICAL ABSTRACT



INTRODUCTION

The development of mining has become very important with the increase in industrialization. However, with the industrial revolution, mining and operating activities have caused the environment to be more polluted (Abdul-Wahab & Marikar 2012). Recently, environmental pollution emerging with the development of mining has reached important dimensions in the world. The residue wastes, named as tailings, as a result of mining activities are a threat to the health of nearby communities and the environment (Goltz & Barnwal 2019). Therefore, it is very important to dispose of this type of mining tailings safely.

Gold mine tailings (GMT) are the ore waste of gold mines and are typically a mud-like material. Although GMT are stored in waste dams, the amount of the tailings is increasing day by day with the development of gold mining. Thus, the treatment of GMT is urgent.

Porous carbon materials have found great interest in many applications due to their surface areas and physico-chemical properties. Porous carbon materials can be classified into three main groups based on their pore diameters: microporous, mesoporous, and macroporous (Liang *et al.* 2008). Among them, activated porous carbons are one of the most important types of industrial carbons (Manocha 2003). Activated carbon is commonly used in adsorption processes, due to its significant adsorption capacity and thermal stability. However, because of the dominant presence of micropores in its structure, it normally demonstrates low uptake capacity (Tsang *et al.* 2007; Bello & Ahmad 2012; Spagnoli *et al.* 2017). In this sense, recent studies have focused on the synthesis of mesoporous carbon-based adsorbents to improve the adsorption ability of the activated carbon.

Mesoporous carbon materials have a high surface area and ordered mesostructures, and they are used as catalysts, adsorbent, and advanced electronic materials in many scientific disciplines (Liang *et al.* 2008). CMK-n is the most important representative of ordered mesoporous carbon materials. SBA-n type mesoporous silica materials are generally used as templates in the synthesis of CMK-n due to their regular structure. CMK-3 is a diverse replica of the SBA-15, and has the same hexagonal structure (Wang *et al.* 2016). It has been used as adsorbents (Ezzeddine *et al.* 2016), electrocatalysts (Yu *et al.* 2009), and catalysts (Peng *et al.* 2010).

Synthetic dye wastewater is another important problem for the environment and human health. Depending on the diversity of these organic and inorganic synthetic compounds used in dyeing and other processes, the characteristics of the wastewater are different. Synthetic dye wastewaters discharged to surrounding waters reduce the light permeability in the water environment and affect the photosynthetic activity negatively (Correia *et al.* 1994). Moreover, these dyes are difficult to biodegrade due to their synthetic source and complex structure. For this

Downloaded from http://iwaponline.com/wst/article-pdf/83/6/1300/865247/wst083061300.pdf
by guest

reason, it is very significant to develop efficient treatment processes for the adsorption of synthetic dyes from wastewater.

Today, due to the inadequacy of water resources and more controlled discharge standards, industries require highly efficient and economical treatment technologies. In addition, recycling and reuse of treated water is an option (Manu & Chaudhari 2002). Various physical, chemical, and biological techniques such as chemical oxidation, solvent extraction, membrane separation, ion exchange, biodegradation, and adsorption are used for the removal of dyes. The adsorption process supplies an easy and common way to effectively remove dye from wastewaters (Wong *et al.* 2003; Yagub *et al.* 2014; Bilinska *et al.* 2015; Mokhtar *et al.* 2015; Liu *et al.* 2016). Much research has been performed to determine proper and affordable adsorbents for dye removal from wastewater.

Recently, the usage of CMK-3 as an adsorbent in the removal of dye adsorbent has received growing attention due to its perfect textural characteristics (Yu *et al.* 2002). Ezzeddine and colleagues produced CMK-3 from SBA-15 synthesized from pure silica for removal of methylene blue. They revealed that the synthesized CMK-3 sample exhibited very high adsorption capacity (Ezzeddine *et al.* 2016). Liu and co-workers revealed that CMK-3 showed stronger adsorption for Reactive Black 5 adsorption than did other adsorbents due to its open and interconnected pore features (Liu *et al.* 2016). Tripathi *et al.* (2013) noticed that the dye removal capacity of ordered mesoporous carbon is directly proportional to the specific surface area and pore volume. Liu and colleagues revealed that CMK-3 exhibited larger adsorption rates for direct yellow 12 adsorption than the adsorption rates of commercial activated carbon (Liu *et al.* 2009).

In this study, the synthesis of CMK-3 using SBA-15 from GMT and the adsorption properties of the synthesized CMK-3 were investigated for the first time. In addition, two CMK-3 samples were synthesized using SBA-15 from pure silica and Pluronic P123 to compare their structural characterizations and adsorption properties. The synthesized samples were characterized by X-ray diffraction (XRD), N_2 adsorption–desorption, and high-resolution transmission electron microscopy (HRTEM). To determine the adsorption behavior of the prepared samples, the effect of various parameters were studied in detail. Adsorption isotherms and kinetics parameters were also analyzed.

EXPERIMENTAL

Materials and methods

The chemicals used to synthesize SBA-15 and CMK-3 were Pluronic P123 from Aldrich, and tetraethyl orthosilicate (TEOS), hydrochloric acid (HCl), sulfuric acid (H_2SO_4), ethanol, sucrose, and hydrofluoric acid (HF) from Merck. Bromcresol green (BCG) (molar mass 698.02 g·mol^{-1}) was purchased from Merck (Figure 1). GMT were obtained from Bergama Ovacık Gold Mine Treatment Plant, Turkey. It was treated by the alkali fusion process described in a previous study (Yilmaz Sari & Piskin 2015a).

XRD data were measured by a diffractometer (PANalytical X'Pert Pro) equipped with CuKα radiation (45 kV/40 mA). Nitrogen adsorption–desorption measurement was carried out at 77.4 K using a volumetric adsorption system (Micromeritics ASAP 2020). Before the analyses, samples were degassed at 573 K. HRTEM measurements were obtained on a transmission electron microscope (JEOL-2100, 200 kV) with LaB_6 electron source. The elemental concentration of extracted solution obtained from the GMT was analyzed by inductively coupled plasma optical emission spectroscopy (Perkin Elmer Optima 2100 DV). The amounts of Si and Al in the extracted solution were found as 28,330 and 1,150 mg·L^{-1}, respectively, indicating that GMT are rich in SiO_2.

Synthesis of silica template

Silica template SBA-15 was synthesized, for CMK-3 synthesis, from two raw materials, pure silica TEOS and GMT, according to the different procedures described in the literature (Zhao *et al.* 1998; Yilmaz Sari & Piskin 2015a, 2015b). The obtained samples from TEOS and GMT were labeled as S_T and S_{GMT}, respectively.

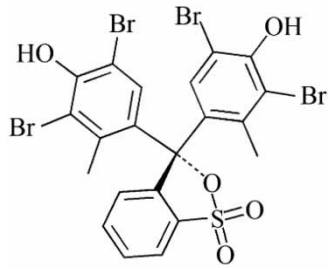


Figure 1 | Molecular structure of BCG.

Downloaded from http://iwaponline.com/wst/article-pdf/83/6/1300/865247/wst083061300.pdf
by guest

Synthesis of CMK-3

Mesoporous carbon CMK-3 was prepared from two different routes. In the first method, S_T or S_{GMT} samples were used as the template, and sucrose was used as the carbon source in the synthesis. Typically, an amount of 1 g of SBA-15 template was dissolved in some distilled water and then mixed with 0.6 g of sucrose and 0.1 g of H_2SO_4. After dissolution, the obtained solution was held in an oven at 100 °C for 6 h, and then the temperature was increased to 160 °C for 6 h. In order to have completely polymerized and carbonized sucrose inside the pores of the template, 2 g of distilled water, 0.05 g of H_2SO_4, and 0.4 g of sucrose were again introduced to the mixture and then it was treated thermally in the same way given above. The samples were then carbonized in argon flow at 900 °C for 4, 5, and 6 h. Finally, the obtained products were washed with 5% HF followed by two more times with ethanol and then dried at 120 °C. Samples obtained from S_T and S_{GMT} were labeled as C_T-x and C_{GMT}-x, respectively, where 'x' denotes the carbonization time.

In the second route, CMK-3 was prepared via the self-assembly method by using P123 copolymer, and the synthesis procedure was conducted based on the study done by Ting *et al.* (2010) with some modifications. Briefly, the P123 copolymer, initially taken as 1.47 g, was first dissolved in distilled water and 2 M HCl with stirring at room temperature. Then, 0.63 g of sucrose was used as a carbon source, and H_2SO_4 was added to the mixture. Then the obtained solution was stirred at room temperature for 30 min. TEOS (2.55 g) was introduced into the mixture under vigorous stirring. Then, the resulting solution was introduced into the autoclave and held at 100 °C for 24 hours. The obtained sample was dried at 100 °C for 6 hours, and then the temperature was set to 160 °C for another 6 hours. After cooling the sample, it was washed with 10% HF and ethanol and dried overnight at 70 °C for removal of the undesired substances. The resulting product was labeled as C_P-x where 'x' denotes the carbonization time.

Adsorption experiments

Batch adsorption experiments were conducted to observe the effect of pH, initial concentration of dye, and contact time. All experiments were done on a Zhicheng incubator shaker with a shaker speed of 150 rpm at room temperature. For the adsorption studies, a 20 mL solution of known dye concentration and 0.006 g adsorbent were placed in an Erlenmeyer. The dye concentrations of the solutions were obtained by a UV-visible spectrophotometer (Perkin Elmer Lambda 35 model) with detecting wavelength at 445 nm. The dye removal and adsorption capacity of the adsorbent were found by the following equations:

$$\text{Dye removal (\%)} = \frac{(C_o - C_t)}{C_o}.100 \quad (1)$$

and

$$q_e = \frac{(C_o - C_e).V}{W} \quad (2)$$

where C_o (mg·L^{-1}), C_t (mg·L^{-1}), and C_e (mg·L^{-1}) are liquid phase equilibrium concentrations of BCG at the start, time t, and at equilibrium, respectively. q_e is the amount of adsorbate adsorbed at equilibrium in mg.g^{-1}, V is the volume in L of the BCG dye solution, and W is the mass in g of the carbon-based adsorbent.

RESULTS AND DISCUSSION

Characterization of the materials

The XRD patterns of S_T, S_{GMT}, and CMK-3 samples synthesized from different procedures are shown in Figure 2. As shown in Figure 2(a), S_T demonstrates a very intense diffraction peak (100) and two obvious peaks (110) and (200), indicating that mesoporous structures form SBA-15 with a 2D hexagonal array and p6mm symmetry with high order (Santhanaraj *et al.* 2011). S_{GMT} only has the (100) reflection, related to the concentration of high electronic density of silanol groups (Si-OH) on the sample surface (Figure 2(b)) (Bérubé & Kaliaguine 2008). C_T-4 and C_T-5 samples have the weak (110) and (200) reflections. An ordered structure occurred in C_T-6, and it has a uniform 2D hexagonally ordered structure, similar to S_T. When the carbon sample was synthesized using the S_{GMT} silica template, the XRD pattern revealed only a broad (100) peak, indicating a less ordered pore structure due to distortion of the hexagonal pore arrangement (Figure 2(b)). This result is similar to those of the S_{GMT}, showing that CMK-3 carbons are a perfect replica of the SBA-15 template. For the C_P-6 and C_P-5 samples, the XRD analysis exhibited three (100, 110, and 200) reflections, which were the well-ordered CMK-3 mesostructure (Figure 2(c)). XRD analysis results showed that the C_T and C_P samples had a more ordered structure with an increase of the carbonization time.

Downloaded from http://iwaponline.com/wst/article-pdf/83/6/1300/865247/wst083061300.pdf
by guest

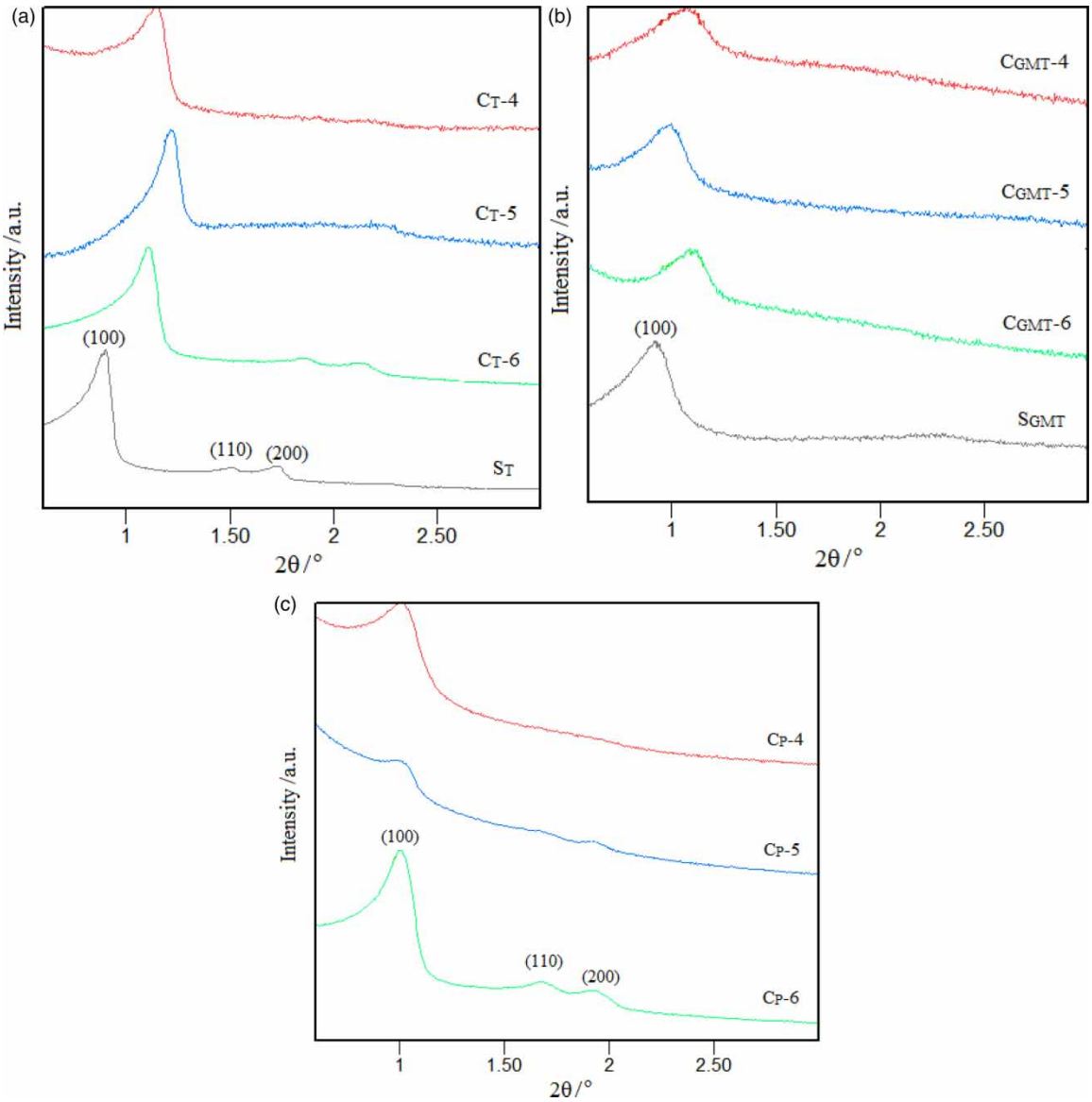


Figure 2 | XRD patterns of (a) C_T-x, (b) C_{GMT}-x, and (c) C_P-x.

Figure 3 shows the N_2 adsorption–desorption isotherms and the related pore size distribution (PSD) curves of the synthesized carbon materials. These isotherms are attributed to a type IV isotherm with typical hysteresis loops in the mesopore range for all the carbon samples. As shown in Figure 3, while C_P-5 has the highest N_2 adsorption, C_{GMT}-5 has the lowest N_2 adsorption. The N_2 adsorption–desorption isotherms of C_T samples showed the largest hysteresis loop due to the strong chemical interaction of the pore wall with N_2. N_2 adsorption–desorption isotherms of C_p-5 demonstrated a smooth continuous increase, implying that it has larger pores. Table 1 presents the structural parameters of the carbon materials calculated from the N_2 adsorption isotherm data. The C_{GMT}-x samples have a smaller surface area and pore volume values than those of the C_T-x. The obtained result is compatible with the XRD, indicating that C_T-x had a more ordered mesoporous structure as compared with C_{GMT}-x. C_T-4 has a higher surface area compared to the other C_T-x samples, and also, C_{GMT}-6 has a higher surface area compared to the other C_{GMT}-x samples. From the table, it can be seen that C_P-5 showed the highest surface area, pore volume, and pore size values compared to the other carbon samples. When the carbonization time increases from 4 to 5 h, specific surface area, pore

Downloaded from http://iwaponline.com/wst/article-pdf/83/6/1300/865247/wst083061300.pdf
by guest

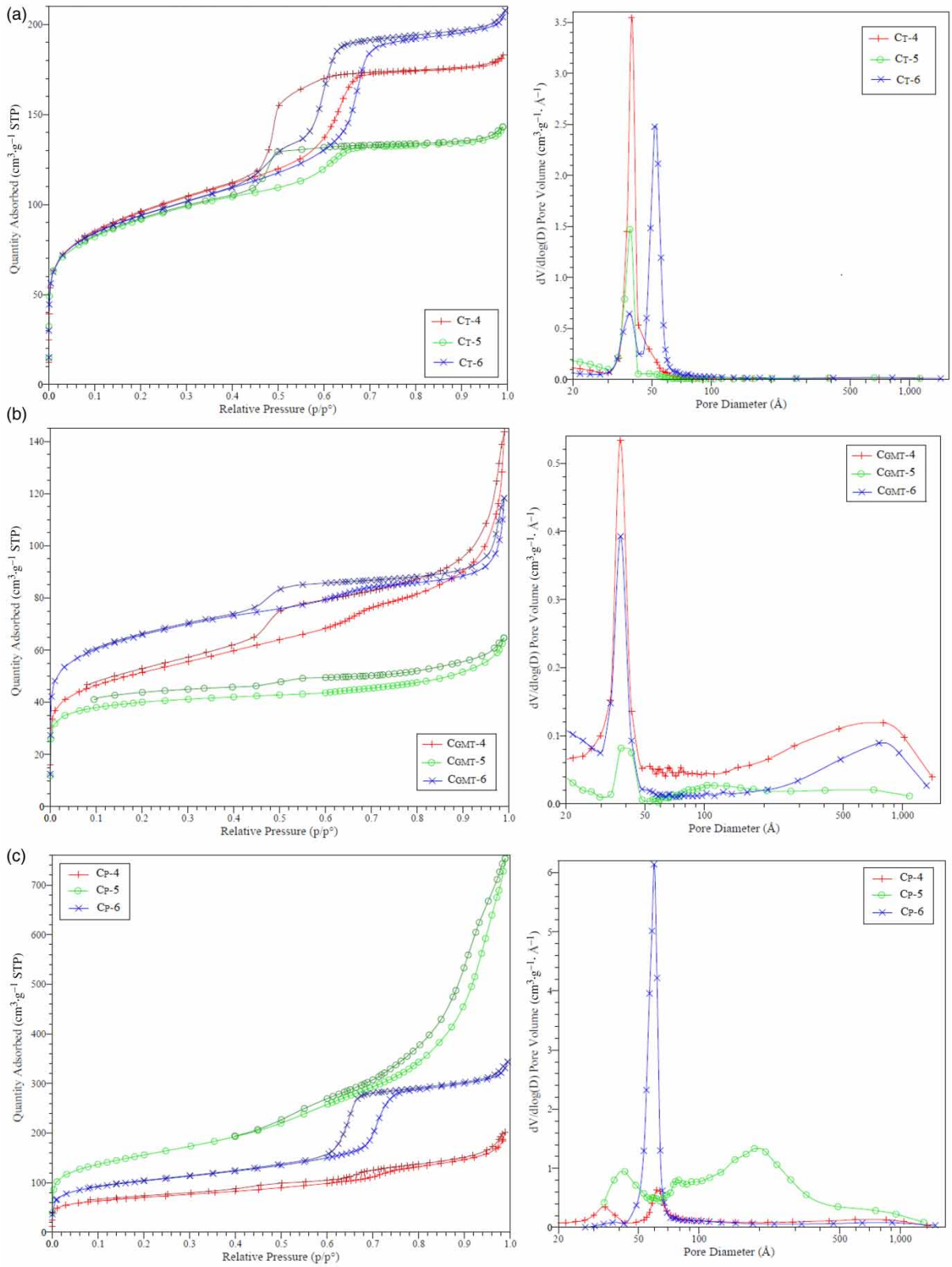


Figure 3 | N_2 adsorption–desorption isotherm and PSD curve of a) (a) C_T-x, (b) C_{GMT}-x, and (c) C_P-x.

Downloaded from http://iwaponline.com/wst/article-pdf/83/6/1300/865247/wst083061300.pdf
by guest

Table 1 | Textural properties of the synthesized carbon samples

Sample	S_{BET} ($m^2 \cdot g^{-1}$)	V_t ($cm^3 \cdot g^{-1}$)	d_{BJH} (nm)
C_T-4	319.56	0.274	3.95
C_T-5	302.38	0.210	3.53
C_T-6	308.29	0.302	4.63
C_{GMT}-4	169.73	0.154	7.02
C_{GMT}-5	124.17	0.086	6.29
C_{GMT}-6	213.20	0.142	5.25
C_P-4	234.46	0.244	6.98
C_P-5	534.00	0.917	11.02
C_P-6	349.01	0.477	6.87

Note: S_{BET}: BET (Brunauer–Emmett–Teller) surface area; V_t: pore volume; d_{BJH}: pore diameter calculated by BJH (Barrett–Joyner–Halenda) model.

volume, and pore size values of C_P increase noticeably. However, the C_T-5 and C_{GMT}-5 have the lowest surface area and pore volume compared to the other C_T-x and C_{GMT}-x samples, respectively. Nevertheless, different trends are observed for all the other samples, and there is no proper relation between samples obtained at different carbonization time in terms of the textural properties. The PSD of C_P-6 exhibited a narrow distribution, while the PSD of C_P-4 and C_P-5 exhibited broad distributions. The large surface area can provide interactive sites for dye molecules within mesoporous samples (Zhuang *et al.* 2009; Chen *et al.* 2018). For this reason, C_T-4, C_{GMT}-6, and C_P-5 with the highest specific surface area were selected as adsorbents for BCG removal in the adsorption studies regardless of whether the adsorbent has an ordered structure.

The HRTEM and TEM images of C_T-4, C_{GMT}-6, and C_P-5 are shown in Figure 4. As can be seen, C_T-4 and C_P-5 samples possess a highly ordered hexagonal array of uniform pore structure (Figure 4(a) and 4(e)). Also, the TEM image of C_T-4 and C_P-5 samples exhibits well-organized mesopores parallel to each other (Figure 4(b) and 4(f)). However, the HRTEM and TEM images of C_{GMT}-6 became obscure, and clearly reveal that this material has a disordered wormlike mesoporous structure (Figure 4(c) and 4(d)). Further, the HRTEM and TEM analysis results also support the conclusion from XRD analysis.

Zeta potential analysis of the C_T-4, C_{GMT}-6, and C_P-5 as a function of solution pH are given in Figure 5. The zeta potentials of the samples continuously decreased with the increase of solution pH. According to measurements, C_T-4, C_{GMT}-6, and C_P-5 have zero charges of around 3, 2.7, and 2.5, respectively, and a positive surface of adsorbents, at pH values below the zero point. Hence, an electrostatic attraction occurred between the anionic dye and positive charges of adsorbent surfaces.

Adsorption studies

The solution pH is one of the important parameters controlling the removal of dyes from wastewater. The pH effect on the removal of BCG was studied by changing the pH value from 2 to 12 while the contact time was kept as 30 min, initial dye concentration was fixed at 25 $mg \cdot L^{-1}$ and the amount of the adsorbent was 0.01 g. As demonstrated in Figure 6, the adsorption capacity of all adsorbents was high at low pH value but then decreased with the increasing pH of the dye solution. In pH = 2, a high electrostatic attraction occurred between dye anions and adsorbent because of the tendency of H^+ ions to interact with the adsorbent surface. The number of negatively charged surface sites on the adsorbent increases with the increase in solution pH so that the adsorbent does not favor the adsorption of anionic dye due to the repulsion (Malik 2004). From Figure 6, the dye removal capacities for all three adsorbents were maximum at the initial pH 2. A similar type of behavior is also reported in the literature for the BCG adsorption with different adsorbents (Shokrollahi *et al.* 2011). According to the results, subsequent adsorption experiments on all carbon-based materials were performed at pH 2.

The effect of contact time and initial dye concentration on the removal of BCG dye on the carbon-based adsorbents was investigated at pH 2, and the amount of adsorbents was 0.006 g for various time intervals. From Figure 7, the adsorption process of all adsorbents was fast in the first 60 min, and after 60 min, increase in contact time exhibited no important effect on the adsorption capacity value and remained nearly unchanged. The reason for the rapid adsorption of BCG at the beginning is the presence of a large number of sorption sites on the surface of the carbon-based adsorbent. When the active sites on the surface are filled, the adsorption rate decreases and eventually reaches equilibrium (Wu *et al.* 2016). It was observed that the adsorption of BCG onto C_T-4 and C_{GMT}-6 exhibited a similar trend. The highest adsorption capacities of C_T-4, C_{GMT}-6, and C_P-5 adsorbents were found as 188.99, 204.57, and 328.74 $mg \cdot g^{-1}$, respectively. It was also seen that the adsorption capacities increased by increasing the dye concentrations for all adsorbents, because more dye molecules can be found at higher initial concentrations. This leads to a greater propellant to accomplish the resistance of mass

Downloaded from http://iwaponline.com/wst/article-pdf/83/6/1300/865247/wst083061300.pdf
by guest

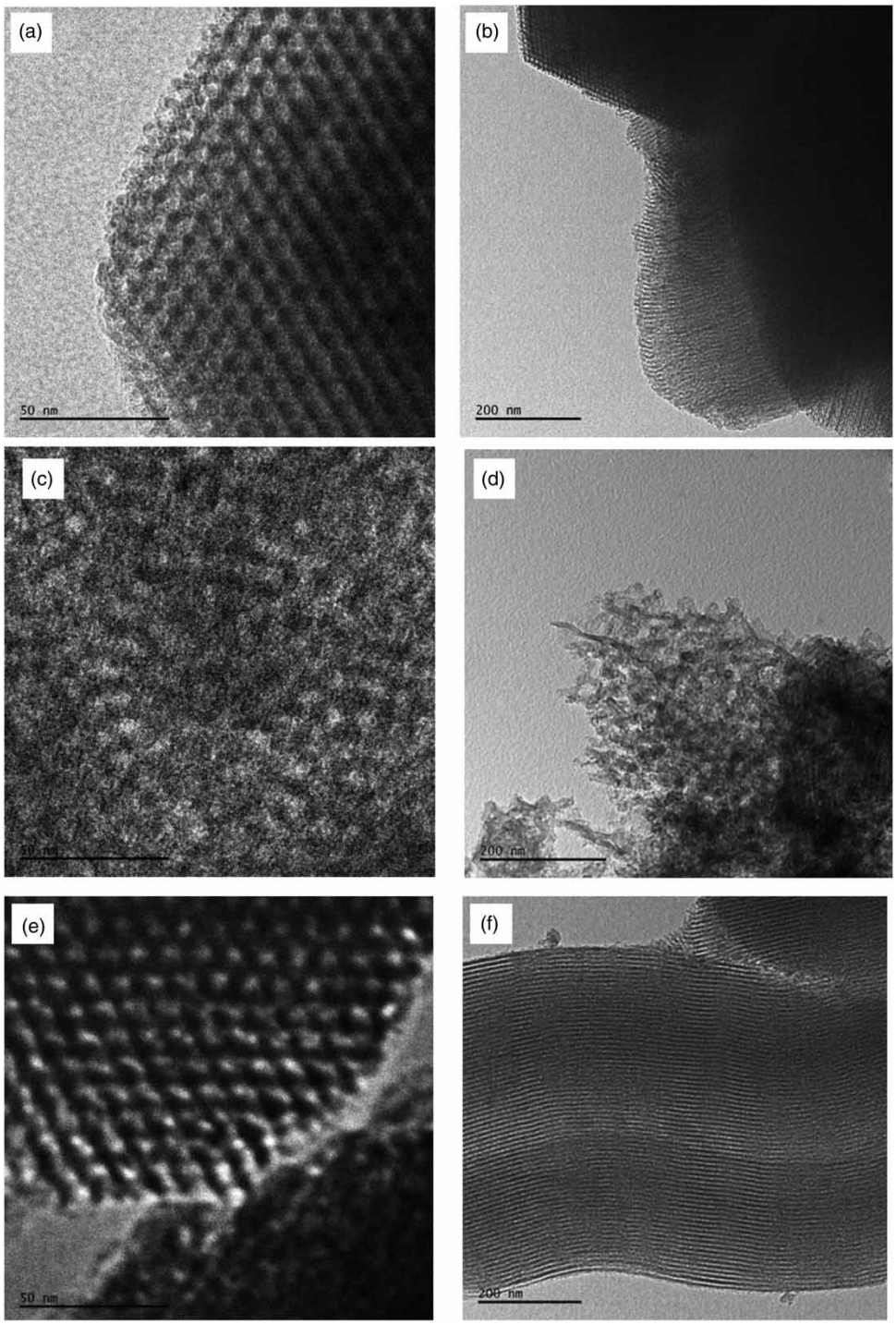


Figure 4 | HRTEM images of (a) C_T-4, (c) C_{GMT}-6, and (e) C_P-5, and TEM images of (b) C_T-4, (d) C_{GMT}-6, and (f) C_P-5 mesoporous carbons.

transfer of the dye among aqueous and solid phases (Mohammadi *et al.* 2011). It was noted that BCG was adsorbed the fastest on the C_P-5 surface according to the C_T-4 and C_{GMT}-6 adsorbents because of the structural properties of C_P-5.

The comparison of the maximum adsorption capacity of dye onto adsorbents synthesized from various wastes is presented in Table 2. The C_{GMT}-6 has very high adsorption capacity as compared to the other samples synthesized from different wastes reported in the literature.

Downloaded from http://iwaponline.com/wst/article-pdf/83/6/1300/865247/wst083061300.pdf
by guest

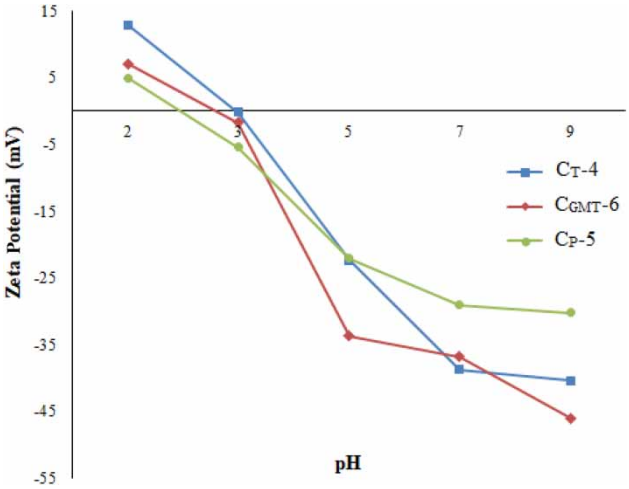


Figure 5 | Zeta potential of C_T-4, C_{GMT}-6 and C_P-5 as a function of pH.

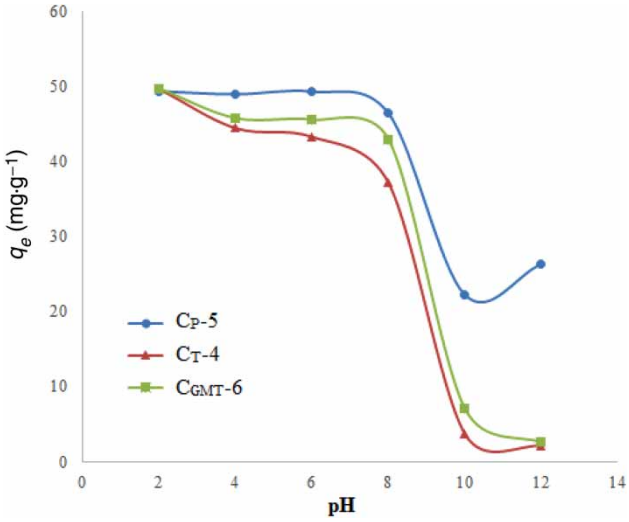


Figure 6 | The effect of solution pH on dye removal (contact time = 30 min, initial dye concentration = 25 mg·L^{-1} and amount of the adsorbent = 0.01 g).

Adsorption kinetics

The kinetics of sorption is a significant factor for the design of a suitable adsorption process (McManamon *et al.* 2012). The various kinetic models were applied for a better understanding of the mechanism of dye adsorption on the adsorbent. The pseudo-first-order model is described below (Mathew & Tandon 1977):

$$\log(q_e - q_t) = \log q_e - \frac{k_1 t}{2.303} \quad (3)$$

where q_e and q_t (mg.g^{-1}) are adsorption capacities at equilibrium and time t, respectively, and k_1 (min^{-1}) is a constant of pseudo-first-order (Harinath *et al.* 2017). The slope and the intercept of the plot of $\log(q_e - q_t)$ versus t were obtained to find k_1 and q_e.

The pseudo-second-order equation can be explained in a linear form as follows (Yang *et al.* 2011; Yan *et al.* 2015):

$$\frac{t}{q_t} = \frac{1}{k_2 q_e^2} + \frac{t}{q_e} \quad (4)$$

where k_2 (g·mg^{-1}·min^{-1}) is a constant. The slope and the intercept of the plot of t/q_t versus t were obtained to find k_2 and q_e.

The adsorption kinetic plots are presented in Figure 8, and the calculated model parameters for all carbon-based adsorbents are summarized in Table 3. Comparison of the estimated adsorption capacity ($q_{e,exp}$) and the correlation coefficient (R^2) values of the kinetic models revealed that the best fit of experimental data was to the pseudo-second-order. The R^2 values of the pseudo-second-order model were higher than the other models. The q_e values and the experimental equilibrium sorption capacities were close to each other for all adsorbents. However, both the pseudo-first and pseudo-second orders cannot determine the mechanism of diffusion. Therefore, the intra-particle diffusion model recommended by Weber and Morris (Weber & Morris 1963) was used to analyze the kinetic parameters to determine if the intra-particle diffusion is a rate-limiting step in the adsorption of BCG on the adsorbent. The intra-particle diffusion model is expressed by the following formula:

$$q_t = k_{id} t^{0.5} + C \quad (5)$$

where k_{id} (mg.g^{-1}·min$^{-1/2}$) is a constant (Harinath *et al.* 2017). C (mg·g^{-1}) value provides knowledge about the thickness of the boundary layer. When a straight plot of q_t versus $t^{0.5}$ passes through the origin, the adsorption process is found to be controlled by intra-particle diffusion only (Zolgharnein & Rastgordani 2018). The intra-particle diffusion plots for all adsorbents are given in Figure 8(c), and the calculated parameters are summarized in Table 3. All intra-particle diffusion plots appear to be divided into two regions (boxes 'a' and 'b' shown in the figure) during the adsorption process, and these plots do not cross the origin, showing that the intra-particle diffusion is not rate-limiting. The first linear region (a) indicates the external mass transfer and diffusion of the dye molecules to active sites on the surface of the adsorbents, while the subsequent

Downloaded from http://iwaponline.com/wst/article-pdf/83/6/1300/865247/wst083061300.pdf
by guest

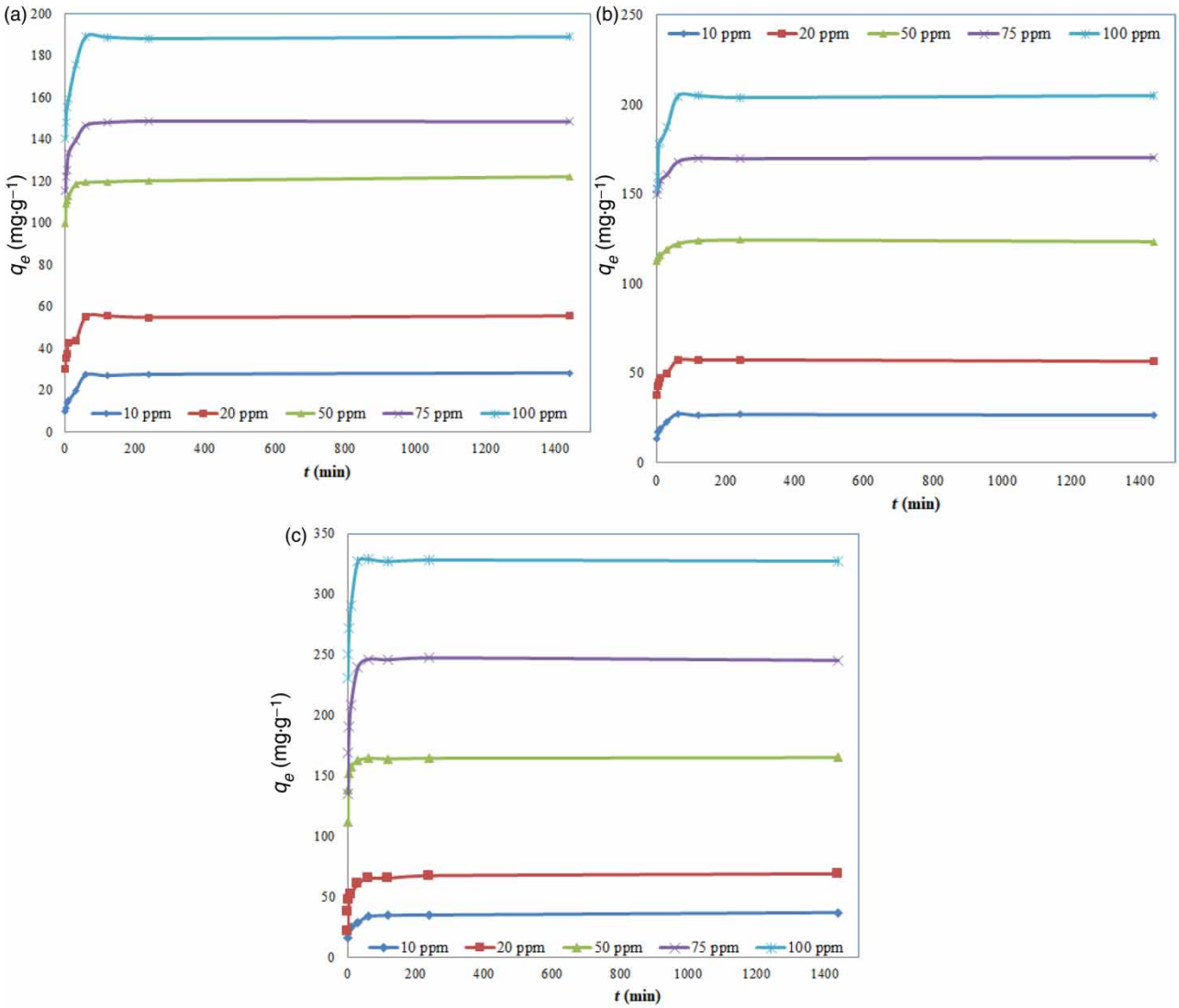


Figure 7 | The effect of contact time and initial dye concentration on BCG adsorption on (a) C_T-4, (b) C_{GMT}-6, and (c) C_P-5 (pH = 2 and amount of adsorbents = 0.006 g).

Table 2 | Comparison of the maximum adsorption capacity of dye onto mesoporous samples from various wastes

Adsorbents	Dye	Adsorption capacity (mg·g^{-1})	Reference
Mesoporous activated carbon fibers synthesized from denim fabric waste	Remazol Brilliant Blue R	292	Silva *et al.* (2018)
C_{GMT}	BCG	204.57	In this study
Mesoporous silica from coal gasification fine slag	Methylene Blue	140.57	Liu *et al.* (2019)
Mesoporous silica from elephant grass	Methylene Blue	123.5	Akpotu & Moodley (2018)
Mesoporous materials using waste quartz	Methylene Blue	96.9	Hong *et al.* (2014)
Mesoporous silica from elephant grass	Methyl Orange	83.3	‘

Downloaded from http://iwaponline.com/wst/article-pdf/83/6/1300/865247/wst083061300.pdf
by guest

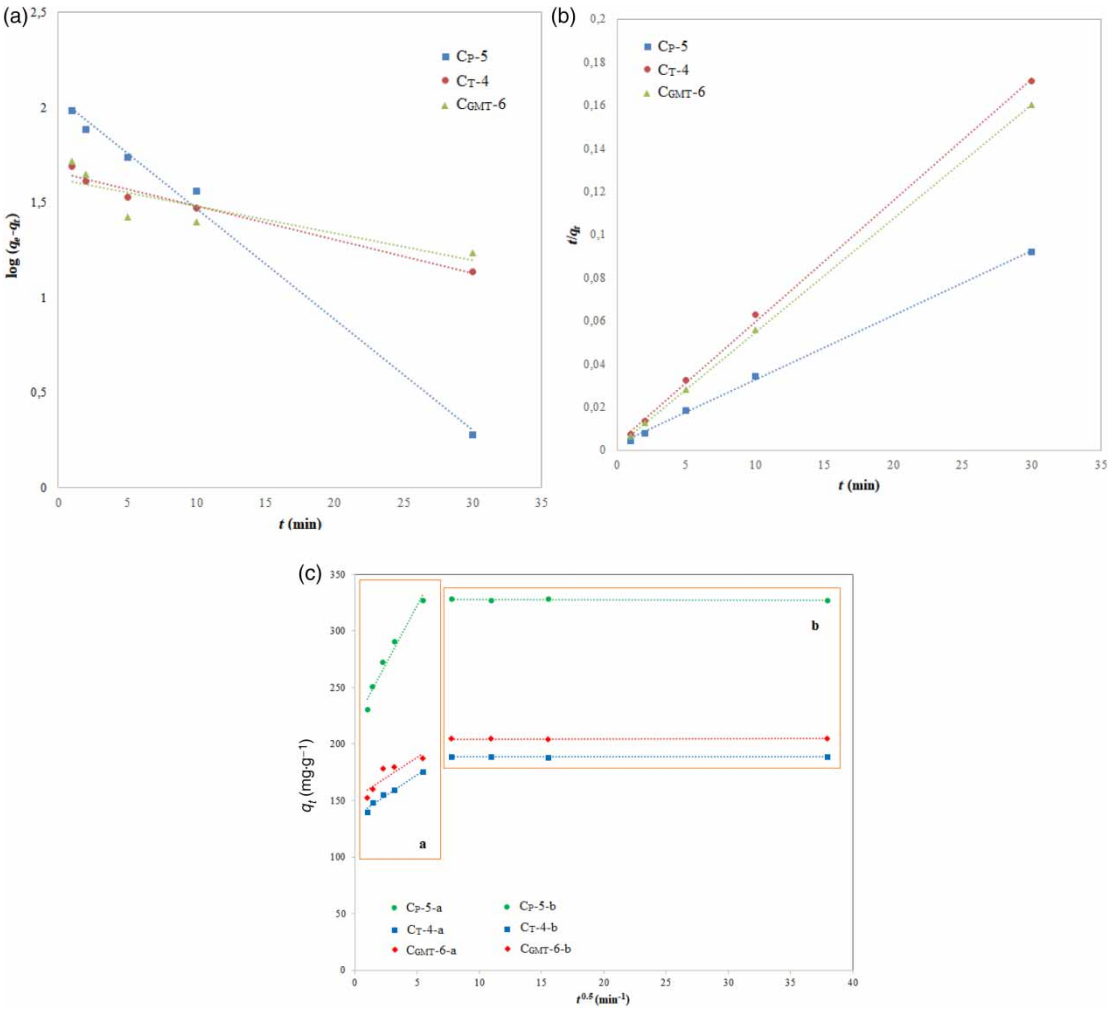


Figure 8 | Adsorption plots (a) pseudo-first-order, (b) pseudo-second-order, and (c) intra-particle diffusion. Conditions: adsorbent dose 0.006 g/20 mL, pH = 2.

Table 3 | Adsorption kinetic parameters of BCG at 100 ppm initial concentration for all of the adsorbents

		Samples		
Models	**Parameters**	**C_T-4**	**C_{GMT}-6**	**C_P-5**
Pseudo-first-order	q_e (mg·g^{-1})	45.38	41.82	111.53
	k_1 (min^{-1})	0.041	0.033	0.134
	R^2	0.978	0.747	0.994
Pseudo-second-order	q_e (mg·g^{-1})	178.57	188.68	333.33
	k_2 (g·mg^{-1}·min^{-1})	0.010	0.015	0.003
	R^2	0.999	1.000	0.999
Intra-particle diffusion model	$k_{id\text{-}a}$ (mg·g^{-1}·min$^{-1/2}$)	7.303	7.241	20.500
	R^2	0.970	0.783	0.963
	C_a (mg·g^{-1})	136.24	152.23	219.52
	$k_{id\text{-}b}$ (mg·g^{-1}·min$^{-1/2}$)	0.003	0.013	− 0.028
	R^2	0.007	0.116	0.201
	C_b (mg·g^{-1})	188.62	204.37	328.30
Experimental	$q_{e,exp}$ (mg·g^{-1})	175.378	187.38	326.85

Downloaded from http://iwaponline.com/wst/article-pdf/83/6/1300/865247/wst083061300.pdf
by guest

region (b) was attributed to the final equilibrium stage for which diffusion begins to slow down because of low dye concentration remaining in the solution. From the table, it was seen that high C values indicate the greater boundary layer effect. The R^2 values for the region 'a' seem to be the lowest for C_{GMT}-6 adsorbent. This may be the result of repulsive forces between the adsorbent and dye molecules

Adsorption isotherms

The adsorption isotherm models represent the relations between the concentration of adsorbate on the solid phase and the liquid phase equilibrium concentration of the adsorbate (Lata *et al.* 2007; Yan *et al.* 2015). In this study, Langmuir, Freundlich, and Temkin isotherms were used to better describe the adsorption process.

The Langmuir model supposes that the adsorption process is a single-layered adsorption mechanism (Langmuir 1916). The Langmuir model is presented as:

$$q_e = \frac{q_m \times K_L \times C_e}{(1 + K_L C_e)} \tag{6}$$

where q_m (mg·g^{-1}) is the maximum uptake capacity, K_L is a constant, and C_e is the equilibrium adsorbate concentration (Zhang *et al.* 2017).

The Freundlich model explains multilayer and reversible adsorption and presumes a heterogeneous adsorbent surface as below:

$$q_e = K_F C_e^{1/n} \tag{7}$$

where K_F is a constant and n is the heterogeneity factor (Freundlich 1906).

The Temkin isotherm represents adsorbent–adsorbate molecule interactions on the adsorption isotherm. An assumption is made that as surface coverage increases, the heat of adsorption of all molecules in the layer decreases linearly (Mall *et al.* 2006). The model equation is given by:

$$q_e = B \ln K_T + B \ln C_e \tag{8}$$

where K_T is the isotherm constant, and B is a constant associated with the adsorption heat.

The obtained parameters derived from all isotherm models are summarized in Table 4. Figure 9 presents the plots of Langmuir, Freundlich, and Temkin models of all carbon-based adsorbents. According to the results of the dye adsorption isotherm experiments, the obtained parameters of C_T-4 and C_{GMT}-6 demonstrate a fitting with the Temkin model, having R^2 values of 0.985 and 0.990 with the heat of sorption values of 47.96 and 55.47, respectively. They also fit the Langmuir isotherm with correlation coefficients 0.979 and 0.980, and the maximum uptake capacity of C_T-4 and C_{GMT}-6, attributed to the complete monolayer coverages, is calculated to be 232.56 and 277.78 mg·g^{-1}. For C_P-5 adsorbent, the Temkin isotherm with $R^2 = 0.980$ with the heat of sorption value 250.54 presents a better fitting of experimental data than Freundlich and Langmuir models.

Reusability of the adsorbents

The regeneration for repeated reuse of the adsorbent is very important for commercial applications. The abilities of the regeneration of the adsorbent were determined in four consecutive adsorption–desorption cycles. After the adsorption process was complete under the optimum conditions, the loaded adsorbents were treated with 0.1 M NaOH. After the regeneration was completed, the adsorbents were mixed again with a fresh NaOH solution, and the second adsorption cycle was carried out. The effect of recycle times on the adsorption capacities of C_T-4, C_{GMT}-6, and C_P-5 is shown in Figure 10. From the figure, the regenerated adsorbents can be used repeatedly at least four times with no evident performance loss. The percentage of decrease in the adsorption capacities of C_T-4, C_{GMT}-6, and C_P-5 after the

Table 4 | The adsorption isotherm model parameters for all adsorbents

	Langmuir			Freundlich			Temkin		
Adsorbent	q_m (mg·g^{-1})	K_L (L·mg^{-1})	R^2	n	K_F (L·mg^{-1})	R^2	B	K_T (L·mg^{-1})	R^2
C_T-4	232.558	0.077	0.979	1.758	23.241	0.968	47.955	0.9313	0.985
C_{GMT}-6	277.778	0.069	0.980	1.629	23.855	0.957	55.467	0.902	0.990
C_P-5	–	− 0.372	0.460	0.678	217.087	0.918	250.54	2.608	0.980

Downloaded from http://iwaponline.com/wst/article-pdf/83/6/1300/865247/wst083061300.pdf
by guest

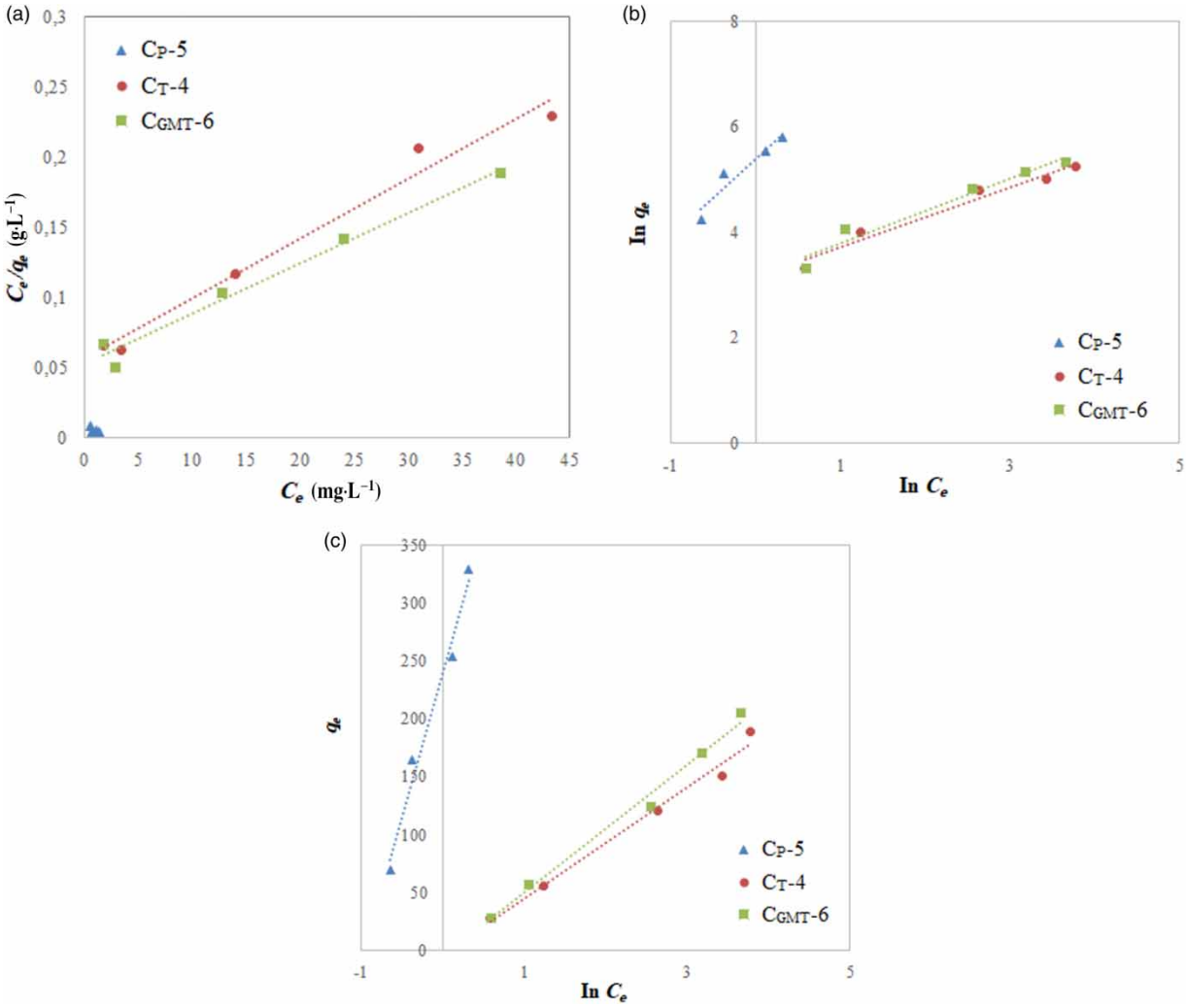


Figure 9 | (a) Langmuir, (b) Freundlich, and (c) Temkin isotherm curve for dye removal. Conditions: adsorbent dose 0.006 g/20 mL, pH = 2.

four cycles were found as 9.4%, 7.8%, and 5.8%, respectively. Results of the reusability study indicated that all adsorbents could be recycled for BCG adsorption, and the adsorbents can be reused.

CONCLUSION

In this study, the removal of BCG dye by CMK-3 synthesized from GMT (C_{GMT}) was studied. Also, two mesoporous carbons, CMK-3 synthesized using SBA-15 from pure silica (C_T) and CMK-3 synthesized by a one-pot route mixing with Pluronic P123 (C_P), were prepared for comparison purposes. Different carbonization times were applied to all synthesized samples, and the samples with the highest surface area were selected as an adsorbent (C_T-4, C_{GMT}-6, and C_P-5) regardless of whether the adsorbent has an ordered structure. The following key points can be drawn from this study:

- The adsorption capacities of the adsorbents are generally decreased by the increased pH of the dye solution. The optimum pH value was selected as 2.
- The adsorption of BCG onto C_T-4 and C_{GMT}-6 adsorbents followed a similar trend.
- Equilibrium data were fitted to the Temkin and Langmuir isotherm model for C_T-4 and C_{GMT}-6.
- The adsorption kinetics of dye onto all adsorbents were best described by a second-order kinetic model.
- The adsorption capacity of C_T-4, C_{GMT}-6, and C_P-5 was found to be 188.99, 204.57, and 328.74 $mg{\cdot}g^{-1}$, respectively, at an initial concentration of 100 ppm.

Downloaded from http://iwaponline.com/wst/article-pdf/83/6/1300/865247/wst083061300.pdf
by guest

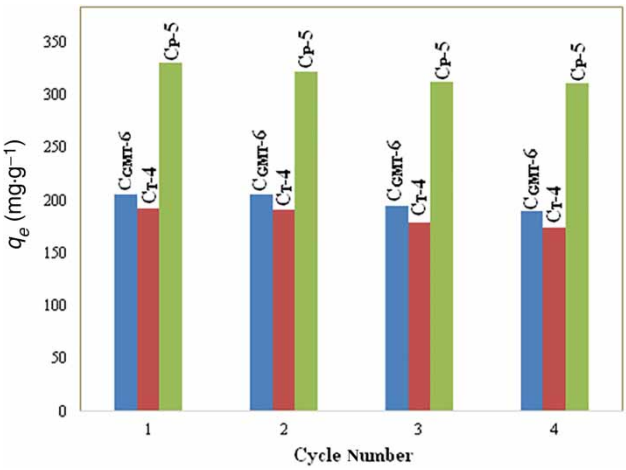


Figure 10 | Reusability studies of the adsorbents after four cycles.

- All adsorbents exhibited excellent reusability during four adsorption–desorption cycles.

Based on these results, it was observed that the C_{GMT} has promising adsorption capacity for BCG removal as a low-cost alternative to C_T.

DATA AVAILABILITY STATEMENT

All relevant data are included in the paper or its Supplementary Information.

REFERENCES

Abdul-Wahab, S. A. & Marikar, F. A. 2012 The environmental impact of gold mine: pollution by heavy metals. *Central European Journal of Engineering* **2** (2), 304–313.

Akpotu, S. O. & Moodley, B. 2018 Effect of synthesis conditions on the morphology of mesoporous silica from elephant grass and its application in the adsorption of cationic and anionic dyes. *Journal of Environmental Chemical Engineering* **6** (4), 5341–5350.

Bello, O. S. & Ahmad, M. A. 2012 Coconut (*Cocos nucifera*) shell based activated carbon for the removal of malachite green dye from aqueous solutions. *Separation Science and Technology* **47**, 903–912.

Bérubé, F. & Kaliaguine, S. 2008 Calcination and thermal degradation mechanisms of triblock copolymer template in SBA-15 materials. *Microporous and Mesoporous Materials* **115** (3), 469–479.

Bilinska, L., Gmurek, M. & Ledakowicz, S. 2015 Application of advanced oxidation technologies for decolorization and mineralization of textile wastewaters. *Journal of Advanced Oxidation Technologies* **18**, 185–194.

Chen, J., Sheng, Y., Song, Y., Chang, M., Zhang, X., Cui, L., Meng, D., Zhu, H., Shi, Z. & Zou, H. 2018 Multimorphology mesoporous silica nanoparticles for dye adsorption and multicolor luminescence applications. *ACS Sustainable Chemistry & Engineering* **6**, 3533–3545.

Correia, V. M., Stephenson, T. & Judd, S. J. 1994 Characterisation of textile wastewaters – a review. *Environmental Technology* **15**, 917–929.

Ezzeddine, Z., Batonneau-Gener, I., Pouilloux, Y. & Hamad, H. 2016 Removal of methylene blue by mesoporous CMK-3: kinetics, isotherms and thermodynamics. *Journal of Molecular Liquids* **223**, 763–770.

Freundlich, H. 1906 Over the adsorption in solution. *Journal of Physical Chemistry* **57**, 1100–1107.

Goltz, J. & Barnwal, P. 2019 Mines: the local wealth and health effects of mineral mining in developing countries. *Journal of Development Economics* **139**, 1–16.

Harinath, Y., Reddy, D. H. K., Sharma, L. S. & Seshaiah, K. 2017 Development of hyperbranched polymer encapsulated magnetic adsorbent (Fe_3O_4@ SiO_2–NH_2-PAA) and its application for decontamination of heavy metal ions. *Journal of Environmental Chemical Engineering* **5**, 4994–5001.

Hong, J. M., Lin, B., Jiang, J. S., Chen, B. Y. & Chang, C. T. 2014 Synthesis of pore-expanded mesoporous materials using waste quartz sand and the adsorption effects of methylene blue. *Journal of Industrial and Engineering Chemistry* **20** (5), 3667–3671.

Langmuir, I. 1916 The constitution and fundamental properties of solids and liquids. Part I. Solids. *Journal of the American Chemical Society* **38**, 2221–2295.

Lata, H., Garg, V. & Gupta, R. 2007 Removal of a basic dye from aqueous solution by adsorption using *Parthenium hysterophorus*: an agricultural waste. *Dyes and Pigments* **74**, 653–658.

Liang, C., Li, Z. & Dai, S. 2008 Mesoporous carbon materials: synthesis and modification. *Angewandte Chemie* **47**, 3696–3717.

Liu, F., Wang, J., Li, L., Shao, Y., Xu, Z. & Zheng, S. 2009 Adsorption of direct yellow 12 onto ordered mesoporous carbon and activated carbon. *Journal of Chemical and Engineering Data* **54** (11), 3043–3050.

Liu, F., Guo, Z., Ling, H., Huang, Z. & Tang, D. 2016 Effect of pore structure on the adsorption of aqueous dyes to ordered mesoporous carbons. *Microporous and Mesoporous Materials* **227**, 104–111.

Liu, S., Chen, X., Ai, W. & Wei, C. 2019 A new method to prepare mesoporous silica from coal gasification fine slag and its application in methylene blue adsorption. *Journal of Cleaner Production* **212**, 1062–1071.

Malik, P. 2004 Dye removal from wastewater using activated carbon developed from sawdust: adsorption equilibrium and kinetics. *Journal of Hazardous Materials* **113**, 81–88.

Mall, I. D., Srivastava, V. C. & Agarwal, N. K. 2006 Removal of Orange-G and Methyl Violet dyes by adsorption onto bagasse fly ash – kinetic study and equilibrium isotherm analyses. *Dyes and Pigments* **69**, 210–223.

Manocha, S. M. 2003 Porous carbons. *Sadhana* **28**, 335–348.

Manu, B. & Chaudhari, S. 2002 Anaerobic decolorisation of simulated textile wastewater containing azo dyes. *Bioresource Technology* **82**, 225–231.

Downloaded from http://iwaponline.com/wst/article-pdf/83/6/1300/865247/wst083061300.pdf
by guest

Mathew, J. & Tandon, S. N. 1977 A radiochemical study of the kinetics of ion-exchange on zirconium antimonate. *Canadian Journal of Chemistry* **55**, 3857–3861.

McManamon, C., Burke, A. M., Holmes, J. D. & Morris, M. A. 2012 Amine-functionalised SBA-15 of tailored pore size for heavy metal adsorption. *Journal of Colloid and Interface Science* **369**, 330–337.

Mohammadi, N., Khani, H., Gupta, V. K., Amereh, E. & Agarwal, S. 2011 Adsorption process of methyl orange dye onto mesoporous carbon material–kinetic and thermodynamic studies. *Journal of Colloid and Interface Science* **362**, 457–462.

Mokhtar, N., Lau, W., Ng, B., Ismail, A. & Veerasamy, D. 2015 Preparation and characterization of PVDF membranes incorporated with different additives for dyeing solution treatment using membrane distillation. *Desalination and Water Treatment* **56**, 1999–2012.

Peng, L., Philippaerts, A., Ke, X., Van Noyen, J., De Clippel, F., Van Tendeloo, G., Jacobs, P. A. & Sels, B. F. 2010 Preparation of sulfonated ordered mesoporous carbon and its use for the esterification of fatty acids. *Catalysis Today* **150** (1–2), 140–146.

Santhanaraj, D., Suresh, C., Gurulakshmi, M., Sasirekha, N. R. & Shanthi, K. 2011 Structural and catalytic properties of V-SBA-15 for the vapor phase oxidation of diphenylmethane. *Reaction Kinetics, Mechanisms and Catalysis* **104**, 399–415.

Shokrollahi, A., Alizadeh, A., Malekhosseini, Z. & Ranjbar, M. 2011 Removal of bromocresol green from aqueous solution via adsorption on *Ziziphus nummularia* as a new, natural, and low-cost adsorbent: kinetic and thermodynamic study of removal process. *Journal of Chemical & Engineering Data* **56**, 3738–3746.

Silva, T. L., Cazetta, A. L., Souza, P. S., Zhang, T., Asefa, T. & Almeida, V. C. 2018 Mesoporous activated carbon fibers synthesized from denim fabric waste: efficient adsorbents for removal of textile dye from aqueous solutions. *Journal of Cleaner Production* **171**, 482–490.

Spagnoli, A. A., Giannakoudakis, D. A. & Bashkova, S. 2017 Adsorption of methylene blue on cashew nut shell based carbons activated with zinc chloride: the role of surface and structural parameters. *Journal of Molecular Liquids* **229**, 465–471.

Ting, C.-C., Wu, H.-Y., Vetrivel, S., Saikia, D., Pan, Y.-C., Fey, G. T. & Kao, H.-M. 2010 A one-pot route to synthesize highly ordered mesoporous carbons and silicas through organic–inorganic self-assembly of triblock copolymer, sucrose and silica. *Microporous and Mesoporous Materials* **128**, 1–11.

Tripathi, P. K., Liu, M., Gan, L., Qian, J., Xu, Z., Zhu, D. & Rao, N. N. 2013 High surface area ordered mesoporous carbon for high-level removal of rhodamine B. *Journal of Materials Science* **48** (22), 8003–8013.

Tsang, D. C., Hu, J., Liu, M. Y., Zhang, W., Lai, K. C. & Lo, I. M. 2007 Activated carbon produced from waste wood pallets: adsorption of three classes of dyes. *Water, Air, and Soil Pollution* **184**, 141–155.

Wang, X., Wu, S., Li, Z., Yang, X., Su, H., Hu, J., Huo, Q., Guan, J. & Kan, Q. 2016 Cu(II), Co(II), Fe(III) or VO(II) Schiff base complexes immobilized onto CMK-3 for styrene epoxidation. *Microporous and Mesoporous Materials* **221**, 58–66.

Weber, W. J. & Morris, J. C. 1963 Kinetics of adsorption on carbon from solution. *Journal of the Sanitary Engineering Division* **89**, 31–60.

Wong, Y., Szeto, Y., Cheung, W. & McKay, G. 2003 Equilibrium studies for acid dye adsorption onto chitosan. *Langmuir* **19**, 7888–7894.

Wu, X.-L., Shi, Y., Zhong, S., Lin, H. & Chen, J.-R. 2016 Facile synthesis of Fe_3O_4-graphene@ mesoporous SiO_2 nanocomposites for efficient removal of Methylene Blue. *Applied Surface Science* **378**, 80–86.

Yagub, M. T., Sen, T. K., Afroze, S. & Ang, H. M. 2014 Dye and its removal from aqueous solution by adsorption: a review. *Advances in Colloid and Interface Science* **209**, 172–184.

Yan, T., Wang, P. & Wang, L. 2015 Utilization of oxalic acid-modified spent mushroom substrate for removal of methylene blue from aqueous solution. *Desalination and Water Treatment* **55**, 1007–1017.

Yang, X., Guan, Q. & Li, W. 2011 Effect of template in MCM-41 on the adsorption of aniline from aqueous solution. *Journal of Environmental Management* **92**, 2939–2943.

Yilmaz Sari, M. & Piskin, S. 2015a Evaluation of novel synthesis of ordered SBA-15 mesoporous silica from gold mine tailings slurry by experimental design. *Journal of the Taiwan Institute of Chemical Engineers* **46**, 176–182.

Yilmaz Sari, M. & Piskin, S. 2015b The removal of template from SBA-15 samples synthesized from different silica sources. *Journal of Thermal Analysis and Calorimetry* **121**, 1255–1262.

Yu, C., Fan, J., Tian, B., Zhao, D. & Stucky, G. D. 2002 High-yield synthesis of periodic mesoporous silica rods and their replication to mesoporous carbon rods. *Advanced Materials* **14** (23), 1742–1745.

Yu, L., Zhao, C., Long, X. & Chen, W. 2009 Ultrasonic synthesis and electrochemical characterization of V_2O_5/mesoporous carbon composites. *Microporous and Mesoporous Materials* **126** (1–2), 58–64.

Zhang, W., Zhu, Z., Zhang, H. & Qiu, Y. 2017 Selective removal of the genotoxic compound 2-aminopyridine in water using molecularly imprinted polymers based on magnetic chitosan and β-cyclodextrin. *International Journal of Environmental Research and Public Health* **14**, 991.

Zhao, D., Huo, Q., Feng, J., Chmelka, B. F. & Stucky, G. D. 1998 Nonionic triblock and star diblock copolymer and oligomeric surfactant syntheses of highly ordered, hydrothermally stable, mesoporous silica structures. *Journal of the American Chemical Society* **120**, 6024–6036.

Zhuang, X., Wan, Y., Feng, C., Shen, Y. & Zhao, D. 2009 Highly efficient adsorption of bulky dye molecules in wastewater on ordered mesoporous carbons. *Chemistry of Materials* **21**, 706–716.

Zolgharnein, J. & Rastgordani, M. 2018 Optimization of simultaneous removal of binary mixture of indigo carmine and methyl orange dyes by cobalt hydroxide nano-particles through Taguchi method. *Journal of Molecular Liquids* **262**, 405–414.

First received 12 July 2020; accepted in revised form 26 January 2021. Available online 8 February 2021

Downloaded from http://iwaponline.com/wst/article-pdf/83/6/1300/865247/wst083061300.pdf
by guest